Indian Journal of Chemical Technology
Vol. 33, July 2026, pp. 650-660
DOI: 10.56042/ijct.v33i4.19359

# Electrical and electrochemical behaviour of $Ba_{0.5}Sr_{0.5}Co_{0.8}Fe_{0.2}O_{3-\delta}$ : Sintering effect

Hemalata Patra[1], Anup Kumar Swain[2]* & Swadesh Kumar Pratihar[3]

[1]CIPET : Institute of Petrochemicals Technology, B-25, CNI Complex, P.O. Patia, Bhubaneswar, Odisha - 751024, India

[2]Chemical Engineering Department, Indira Gandhi Institute of Technology, Sarang, Dhenkanal, Odisha – 759146, India

[3]Ceramic Engineering Department, National Institute of Technology, Rourkela, Odisha – 769008, India

*E-mail: anup.k.swain@gmail.com

*Received 2 May 2025; accepted 30 June 2026*

Investigations have been carried out on $Ba_{0.5}Sr_{0.5}Co_{0.8}Fe_{0.2}O_{3-\delta}$ (BSCF) perovskite oxides as cathode material for their use in intermediate temperature solid oxide fuel cells (IT-SOFCs). Thermal expansion coefficient (TEC), structural features, electrical conductivity, thermal analysis (weight-loss behaviour), and electrochemical properties were characterized by dilatometry, X-ray diffraction (XRD), DC four-probe measurements, thermogravimetry (TG), and electrochemical impedance spectroscopy (EIS), respectively. The thermal stability of BSCF samples was found to be up to 1100 °C. Efforts have been made to study the influence of sintering profile on the microstructure and electrical conductivity of BSCF samples. The microstructure of the BSCF samples was found to be greatly influenced by the sintering parameters. The micrographs revealed that the samples sintered at lower temperatures possessed a porous structure. The electrochemical behaviour of the BSCF/Samarium doped ceria (SDC)/yttria-stabilized zirconia (YSZ)/SDC/BSCF symmetric cells has been studied as a function of sintering conditions of the BSCF electrode. The observed electrical and electrochemical behaviour of the BSCF samples has been correlated with the electrode processing parameters. The activation energies were found to be 86.94 and 104.22 kJ/mol for the electrodes sintered at 1000 and 1100 °C, respectively.

**Keywords:** BSCF cathode, Electrical and electrochemical behaviour, Microstructure, Sintering profile, Solid oxide fuel cell

## Introduction

Solid oxide fuel cell (SOFC) cathode materials must exhibit a range of properties, such as higher electrical conductivity[1–4], minimal thermal expansion mismatch with the electrolyte[5–7], significant catalytic activity for oxygen reduction[8–11], stability under oxidizing environment[12], and compatibility with other components of the cell[13]. Among these, the catalytic activity for oxygen reduction and compatibility with the electrolyte carry prime importance[14–17].

From a catalytic activity perspective, numerous perovskite oxides have been investigated as potential SOFC cathode materials[14,18–23]. Traditional SOFC cathode material is strontium-doped lanthanum manganite (La,Sr) $MnO_3$ (LSM)[24]. However, its application in IT-SOFCs is limited, due to its low oxygen ion conductivity ($10^{-7}$ S/cm at 900 °C)[25]. In contrast, rare-earth-doped lanthanum ferrites, such as $(La,Sr)(Co,Fe)O_3$ (LSCF), demonstrate a much higher oxygen ion conductivity (0.2 S/cm at 900 °C), making them a popular choice for IT-SOFC cathode material[26,27].

BSCF is a mixed ionic and electronic conductor, characterized by its significant catalytic activity for oxygen reduction and oxygen-ion permeability[28]. It also performs exceptionally well as a cathode with samarium and gadolinium-doped ceria (SDC/GDC) electrolytes[29–35]. However, ceria-based electrolytes are susceptible to reduction in a reducing environment. Therefore, the use of ceria-based electrolytes requires specific protective measures against the reducing environment at the anode side of fuel cells.

On the other hand, zirconia-based electrolytes (especially YSZ) exhibit greater stability in both oxidizing and reducing environments[36]. Additionally, it is important to note that the cobalt-containing cathode materials, including BSCF, are incompatible with YSZ electrolytes. This is due to their reaction with the electrolyte and subsequent formation of an insulating interfacial layer at the working temperature. This significantly reduces the catalytic performance of the electrodes[13,16]. Therefore, BSCF cathode materials cannot be directly applied to YSZ electrolytes. The introduction of a ceria-based buffer layer on the YSZ electrolyte at the cathode side can be one strategy to overcome this issue. However, limited literature has reported the electrochemical performance of BSCF on ceria-based buffer layered YSZ electrolytes[37].

The current investigation involved the synthesis of BSCF powders via a combined ethylene diaminetetraacetic acid (EDTA)-assisted citrate-nitrate solution combustion method. In this technique, EDTA acts as a chelating agent while citric acid serves as a chelating agent and a fuel for combustion. There are two aspects of the present study: (i) fabrication of the symmetric cell consisting of BSCF/SDC/YSZ/SDC/BSCF (this stage required sintering of fabricated bulk and thick film in the temperature range 1000-1100 °C) and (ii) study the electrical and electrochemical behaviours of the sintered BSCF samples and predict cell performance in the application temperature region (650-800 °C). To address both issues, bulk and thick-film samples were sintered at 1000–1100 °C for fabrication, while electrical conductivity and polarization resistance were measured over 650–800 °C. An attempt has been made to assess the electrode's electrical and electrochemical performance from its microstructure and defect chemistry. Morphological studies of the sintered (1050-1100 ℃) samples (bulk and thick film) were useful for assessing their properties. The temperature-dependent weight loss and thermal expansion behaviour reported in the study support the defect-chemistry model used to explain the transport properties. At a very low current density, the catalytic activity of the BSCF cathode was assessed using impedance spectroscopy.

**Experimental Section**

The BSCF powder studied in this manuscript was prepared using the solution combustion technique, in which the stoichiometric amounts of nitrate salts of the required chemical constituents are dissolved in water. Citric acid and EDTA are also added to this prepared nitrate solution. This added citric acid serves as a fuel and also chelates the metal ions. EDTA is used as a chelating agent to avoid preferential precipitation. Upon heating and stirring, the mixed citrate-nitrate-EDTA solution undergoes dehydration followed by gel formation. This gel, upon further heating, undergoes combustion, forming an ash (combustion residue). Further calcination of the combustion residue at a high temperature yielded phase-pure BSCF powder. The calcined powders were ground and granulated with 3 wt.% polyvinyl alcohol (PVA) and then sintered at the temperature range of 1000 to 1100 °C with a soaking time of 2 to 8 h. The detailed procedures regarding synthesis, calcination, granulation, and sintering have been well documented in previously published literatures[29,38].

The phases present in the sintered samples were characterized by X–ray diffractometer (PW1830, Panalytical) with nickel-filtered Cu–$K_\alpha$ radiation ($\lambda$ = 0.15418 nm) in the range (2$\theta$) of 20 to 80°, operated at 35 kV and 30 mA. Weight-loss behaviour and thermal analysis of the calcined powder were studied using a simultaneous thermal analyzer (TGA-DSC, STA 449C, NETZSCH) at a heating rate of 10 °C/min to 800 °C under air.

The granulated powders were molded into rectangular bars (15 mm x 5 mm x 2 mm) at 350 MPa, and then sintered. The sintered samples were used for thermal expansion and electrical conductivity measurements. Thermal expansion was measured in air over a temperature range of 30 to 800 °C using a dilatometer (DIL 402C, NETZSCH) heated at 10 °C/min. While electrical conductivity was measured in open air over the same temperature range using the DC four-probe method, accounting for the effects of sintering temperature and soaking time. The bulk electrical transport behaviour of the BSCF sintered samples was studied in the present investigation. The samples for the study (bulk and thick film) were prepared after post-fabrication sintering at 1000-1100 ℃, while the electrical conductivity and polarization resistance were assessed over the temperature range 650-800 ℃. Ag-paste was used to form electrical contacts between the samples and the platinum leads. The outer two platinum wires served as current leads, while the inner two served as voltage leads. The mounted sample was placed in a horizontal tube furnace, and the sample's resistance was measured using a multimeter (Agilent 34970A Data Acquisition/Switch unit) at 5 °C increments. The sintered sample morphology was studied by scanning electron microscope (SEM) (JSM6480LV, JEOL).

To evaluate the electrochemical properties, symmetrical electrochemical cells were fabricated using porous electrodes and a dense YSZ electrolyte in between them. On both sides of the electrolyte, SDC buffer layers were applied. Pressed along a single axis, YSZ electrolyte disks were sintered at 1550 °C for 4 h in air, then polished and cleaned. The buffer layer on the electrolyte was fabricated by screen printing technique using SDC slurry consisting of a premixed solution of glycerol, ethylene glycol, and isopropyl alcohol. The screen-printed electrolyte samples were then sintered at 1400 °C for 4 h. BSCF

powder was mixed with the premixed solution, and the resulting mixture was ground in a planetary mill. The prepared electrode pastes were symmetrically screen-printed on both sides of the buffer layer applied to the electrolyte, and the resulting cells were sintered at 1000 °C and 1100 °C for 2 h. Subsequently, silver paste was applied to the electrodes, which were then cured at 550 °C for 1 h.

AC electrochemical impedance measurement of the symmetrical cells was carried out using an impedance/gain phase analyzer (SI 1260, Solartron) along with an electrochemical interface (SI 1287, Solartron) in order to examine the effect of the BSCF electrodes' sintering temperature in the range of 650 to 800 °C.

## Results and Discussion

### X-ray diffraction

In this study, XRD was performed on sintered (1100 °C/8 h) samples to assess the phase stability of the synthesized powder at high temperature, which is shown in Fig. 1. From the Rietveld analysis, it is observed that the cubic perovskite structure is well indexed with a lattice parameter of 3.9939 Å, which corresponds well with the previously published data[17]. Crystal structure has been refined assuming a cubic perovskite unit cell with space group Pm3m. The XRD pattern showed no additional peaks beyond BSCF, indicating that BSCF remains stable up to the sintering temperature (1100 °C).

### Thermogravimetric analysis

The TG profile (Fig. 2) of the calcined BSCF powder shows a gradual, slow weight loss over the temperature range of 30 to 400 °C. This weight reduction is primarily due to the desorption of physically adsorbed water and carbon dioxide at 30-200 °C[39,40]. At high temperatures, the composition of BSCF exhibits instability[41]. Weight loss increases rapidly in the temperature range of 400 to 500 °C, after which it decreases. This reduction is due to the loss of the lattice oxygen and could be explained by the following equations[40]:

$$2\,Co_{Co}^{\cdot} + O_{O}^{x} = 2\,Co_{Co}^{x} + V_{o}^{\cdot\cdot} + \frac{1}{2}O_2(g) \quad \ldots (1)$$

$$2\,Fe_{Fe}^{\cdot} + O_{O}^{x} = 2\,Fe_{Fe}^{x} + V_{o}^{\cdot\cdot} + \frac{1}{2}O_2(g) \quad \ldots (2)$$

where, $Co_{Co}^{\cdot}$ & $Fe_{Fe}^{\cdot}$= holes, $Co_{Co}^{x}$ & $Fe_{Fe}^{x}$ = cobalt & ferric ions, $V_{o}^{\cdot\cdot}$= oxygen vacancy, and $O_{o}^{x}$ = oxygen ion. As the temperature exceeds 500 °C, an increasing number of oxygen vacancies are generated due to the thermal loss of lattice oxygen. Simultaneously, to preserve electrical neutrality, the valence states of Co and Fe ions are reduced from 4+ to 3+. As the temperature rises, the equilibrium of the aforementioned equations shifts to the right, leading to increased weight loss[39, 40].

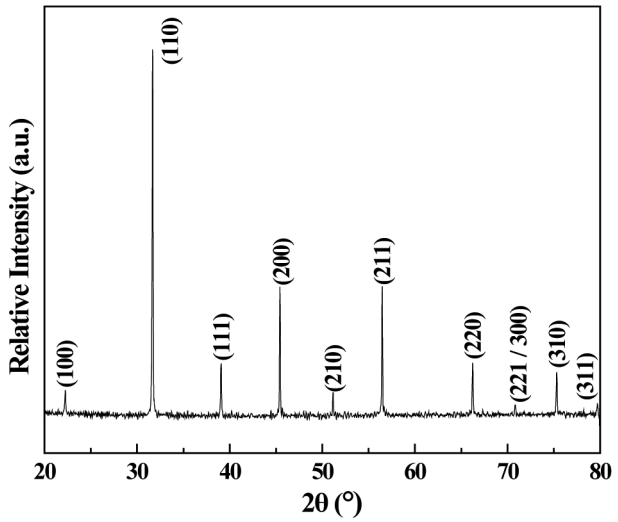


Fig. 1 — X-ray diffraction pattern of sintered BSCF pellets

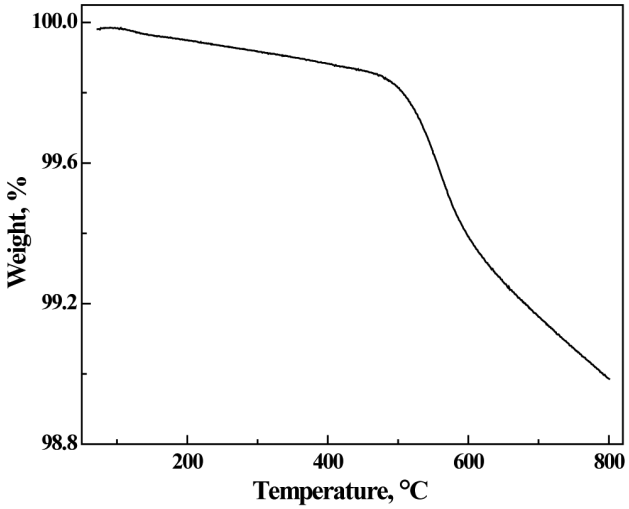


Fig. 2 — Thermogravimetric analysis of BSCF powders

### Thermal expansion behaviour

The thermal expansion property of BSCF, which underwent sintering at 1100 °C for 4 h in the presence of air, is depicted in Fig. 3. The expansion is observed to be linear in the low temperature range of 30 to 500 °C. At higher temperatures in the range 500 – 800 °C, the expansion is observed to be nonlinear, which correlates with lattice oxygen loss. With the increase in temperature, oxygen vacancies

get increased[13]. This can also be validated by the outcomes obtained from TG analysis. Consequently, the loss of lattice oxygen or the formation of vacancies results in the reduction of higher-valence-state B-site cations to lower valence states. When an oxygen ion is lost from the lattice, it creates a repulsive force between the cations. In contrast, the B-site cations undergo a change in valence state to maintain charge neutrality, thereby increasing their size. The unusual lattice expansion observed can be attributed to repulsive forces and changes in cation size. This observation is similar to the findings for cobalt-containing perovskite materials[39]. The specific TEC values are 12.99, 22.48, and 17.48 ($x10^{-6}$/K) over the temperature ranges 30 to 300, 300 to 500, and 30 to 800 °C, respectively. These results indicate that the TEC is predominantly influenced by the higher-temperature range and by the changes in the ionic radius of the metal ions in the lattice[42].

**Microstructural study of BSCF samples**

SEM micrographs of BSCF samples, which underwent sintering at the temperature range of 1000 to 1100 °C for a soaking period of 4 h, are shown in Fig. 4. Samples sintered at temperatures of 1000 and 1050 °C exhibited a porous structure, characterized by interconnected pores (Fig. 4(a) and (b)). Sintering the sample at 1100 °C yielded a dense microstructure with well-defined grain boundaries (Fig. 4(c)). The distribution of grain sizes revealed a broad range. The formation of larger grains can be attributed to the presence of large agglomerates in the powder. The average grain sizes of 3.98±0.5, 6.71±1.5, and 11.84±2.4 μm were recorded at sintering temperatures of 1000, 1050, and 1100 °C, respectively, for a soaking time of 4 h.

SEM micrographs of BSCF samples sintered at a constant temperature of 1100 °C are shown in Fig. 5 as a function of soaking time (2 and 8 h). Shorter soaking times produce a porous microstructure, while longer ones result in a denser one. The average grain sizes measured at a sintering temperature of 1100 °C are 8.88±1.3, 11.84±2.2, and 14.76±2.6 μm for soaking times of 2, 4, and 8 h, respectively. These results suggest that average grain size increases with increasing sintering temperature and soaking time.

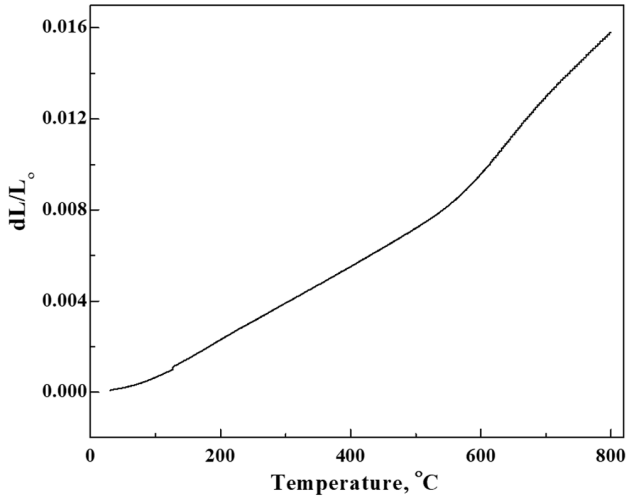


Fig. 3 — Thermal expansion behaviour of BSCF

**Electrical conductivity of BSCF samples**

The temperature dependence of BSCF samples' electrical conductivity as a function of sintering temperature and soaking time is shown in Fig. 6. Previous studies provide a comprehensive explanation of both ionic and electronic conductivities, which are responsible for electrical conductivity[43,44]. A-site of the studied perovskite is occupied by divalent cations (Ba and Sr) while the B-site is occupied by transitional metal cations (Co and Fe). The stable oxidation state of the B-site cations (Co and Fe) is +3. Hence, these oxides could not exist as stoichiometric ones to maintain charge neutrality. The electrical charge neutrality in this oxide is achieved by the formation of an oxygen vacancy (Eq. 3) and an

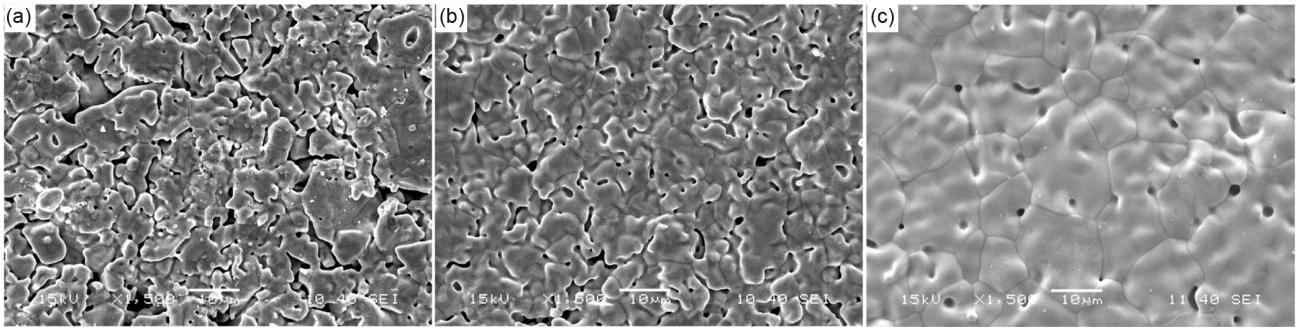


Fig. 4 — Microstructure of BSCF samples sintered at: (a) 1000 °C, (b) 1050 °C, and (c) 1100 °C for a constant soaking period of 4 h

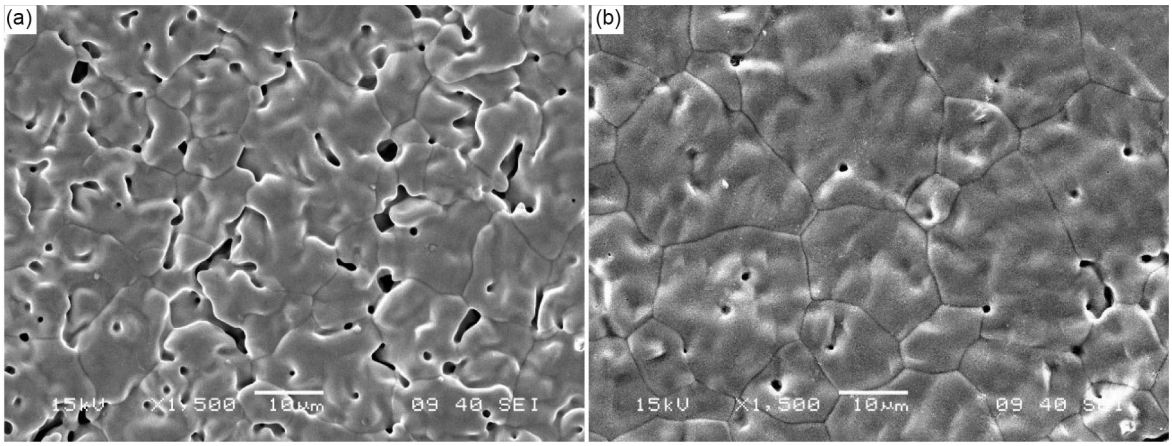


Fig. 5 — Microstructure of BSCF sintered at1100 °C for soaking period of: (a) 2 h and (b) 8 h

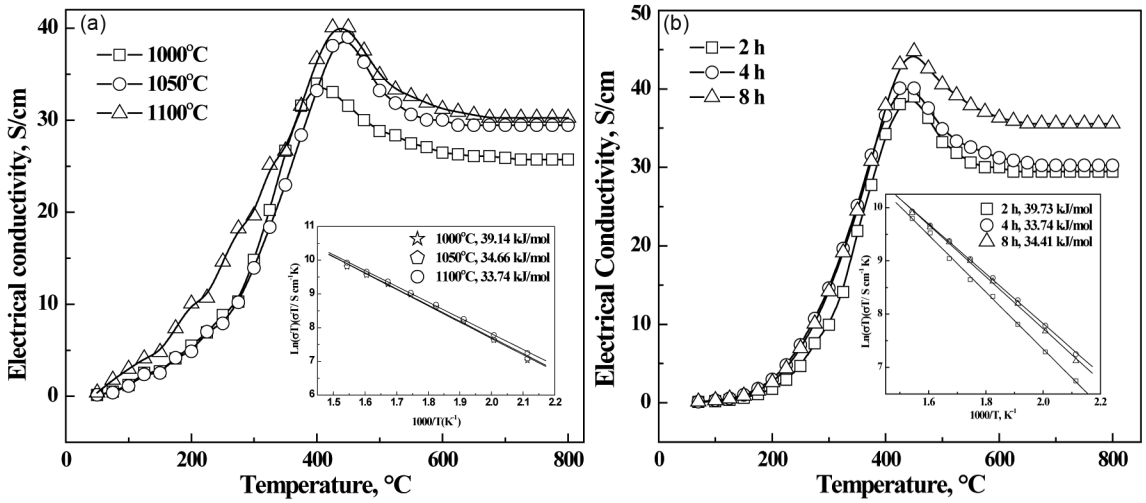


Fig. 6 — Temperature dependence electrical conductivity and conductivity Arrhenius plots as a inset of BSCF: (a) as a function of sintering temperature and (b) as a function soaking time

increase in the oxidation state of the B-site cations. A change in the oxidation state of the B-site transition-metal ions from trivalent to tetravalent state will generate a hole in the oxide structure (responsible for electronic conductivity) (Eqs. 4 and 5). On the other hand, the formation of an oxygen vacancy in these oxides provides the pathway for ionic conduction. Thus, both ionic and electronic conductivities exist in the BSCF samples. The oxygen vacancy and hole concentrations are in equilibrium.

$$O_o^x = \frac{1}{2}O_2(g) + V_o^{\cdot\cdot} + 2e' \quad \ldots (3)$$

$$Co_{Co}^X \Leftrightarrow Co'_{Co} + h^{\cdot} \quad \ldots (4)$$

$$Fe_{Fe}^X \Leftrightarrow Fe'_{Fe} + h^{\cdot} \quad \ldots (5)$$

where, $h^{\cdot}$= missing electron or hole, $e'$ = quasi-free electron, and $Co'_{Co}$ & $Fe'_{Fe}$ = dopant on the normal lattice site.

These oxides undergo thermal reduction with increasing temperature (as explained in the thermogravimetric study and supported by the thermal expansion study), thereby increasing the oxygen vacancy concentration. Oxygen vacancy formation is associated with the creation of electrons. These electrons are trapped with the holes (tetravalent B-site cations), lowering the average oxidation state of the B-site cations and reducing the hole (charge carrier) concentration at temperatures above 500 °C[45]. This decrease in charge-carrier concentration reduces the material's electronic conductivity measured by the DC technique. With a further increase in temperature, the rate of thermal reduction decreases, and the increase in oxygen vacancy concentration enhances ionic conductivity, and thus measured electrical conductivity (electronic conductivity) remains almost constant beyond 600 °C.

The study revealed that conductivity increases with higher sintering temperatures and longer soaking times. The maximum conductivity values recorded were 40.25 and 44.85 S/cm for samples sintered at 1100 °C with soaking times of 4 and 8 h, respectively. Conversely, at sintering temperatures of 1000 and 1050 °C, the conductivities were measured to be 33.02 and 39.02 S/cm, respectively, when the soaking time was held constant at 4 h. The rise in conductivity associated with higher sintering temperatures and extended soaking times can be attributed to the microstructural characteristics and sintered density. Samples sintered at 1000 °C were highly porous, with a density of 66%. This porosity impeded electrical conduction, resulting in lower conductivity values. Earlier discussions have highlighted that the grain size of the samples tends to increase with both sintering temperature and soaking time. This growth in grain size may account for the rise in electrical conductivity observed with higher sintering temperatures and longer soaking periods.

The highest conductivities were recorded at temperatures between 300 and 500 °C, known as the characteristic temperature, which is attributed to a p-type small-polaron hopping mechanism in which electrons hop from $B^{+(n-1)}$ cations to $B^{+n}$ cations via the oxygen bridges[44,45]. The conduction mechanism is inferred from the calculated activation energy, based on Arrhenius-type conduction behaviour at low temperatures. The temperature dependence of conductivity in the low temperature range (below 300 °C) can be analyzed using the Arrhenius equation as follows.

$$\sigma = \left(\frac{A}{T}\right) \exp\left(\frac{-E_a}{KT}\right) \quad \ldots (6)$$

where, σ = electrical conductivity, A = pre-exponential constant, $E_a$ = hopping activation energy, K = Boltzmann's constant, and T = absolute temperature[44,45]. The activation energies in the low-temperature range were found to be between 33.74 and 39.14 kJ/mol, which closely correspond to the literature value[45]. The small increase in activation energy observed in samples sintered for shorter times or at lower temperatures could be attributed to the hindrance to electrical conductivity imposed by porosity or grain boundaries.

**Microstructural study of BSCF electrode**

SEM micrographs of the BSCF electrode on the SDC buffer-layered YSZ electrolyte are shown in Fig. 7, reflecting the influence of sintering temperature. The electrode sintered at 1000 °C for 2 h displayed a porous microstructure with coarse BSCF grains (Fig. 7a), whereas sintering at 1100 °C for 2 h yielded large, interconnected grains, with porosity evident at grain interfaces (Fig. 7b).

**AC impedance studies**

Impedance plots are widely used to understand the various charge-transfer processes at the electrode-electrolyte interface. The impedance spectra of BSCF on SDC buffer-layered YSZ electrolyte is shown in Fig. 8. Fig. 8(a) represents the actual impedance plot of the symmetric cell sintered at 1000 and 1100 °C, measured at 650 °C. Fig. 8(b) represents the change in polarization resistance with measurement temperature. The total resistance offered at the electrode-electrolyte interface is known as polarization resistance ($R_p$). Two phenomena (i) delay in electron/ion transfer and (ii) delay in reactant transport to and from the electrode contributes to the polarization resistance. The former is known as charge-transfer resistance ($R_1$) and the latter is concentration/diffusion polarization ($R_2$), which depends on the diffusion of the reactant species

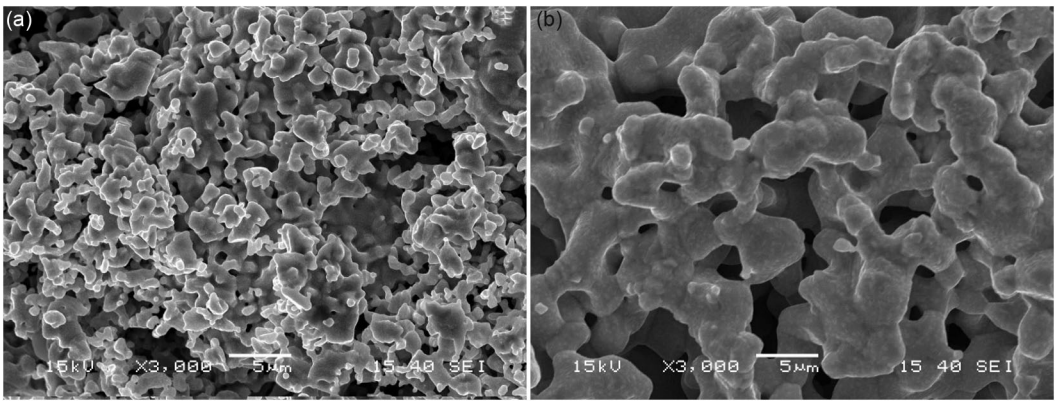


Fig. 7 — SEM micrograph of BSCF electrode on SDC buffer layered YSZ electrolyte as a function of sintering temperature

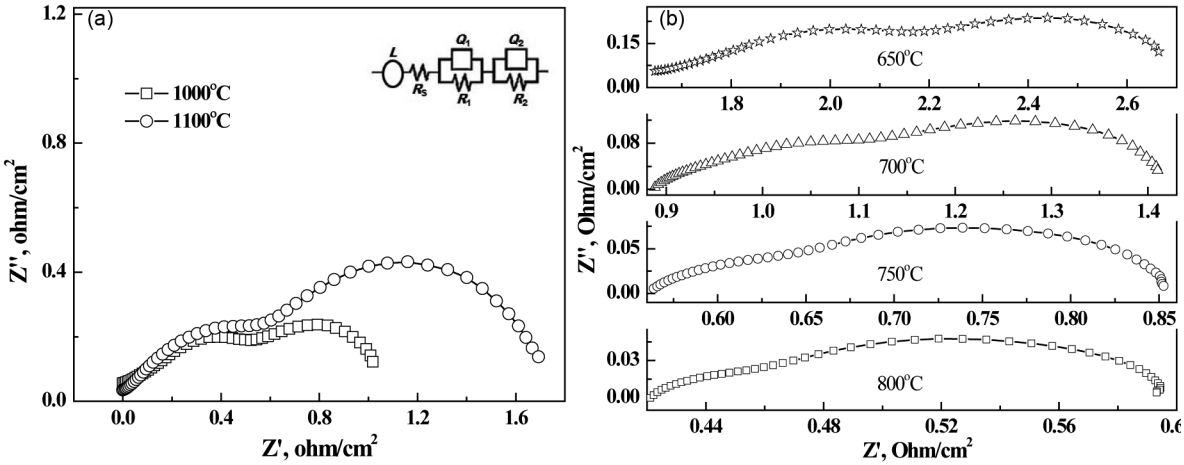


Fig. 8 — Impedance spectra of BSCF electrode on SDC buffer layered YSZ electrolyte: (a) as a function of sintering temperature of the electrode measured at 650 °C and (b) as a function of temperature, electrode sintered at 1000°C [Z' = the real part of the impedance and Z'' = the imaginary part of the impedance]

(oxygen vacancies in this case)[40]. Accordingly, an equivalent circuit representing charge transfer and concentration/diffusion polarization is presented in Fig. 8(a). The electrolyte resistance ($R_s$) and possible contact inductance (L) are also included in the equivalent circuit. However, these two parameters are not important for the present study. As depicted in Fig. 8(a), there is an increase in polarization resistance ($R_p$) corresponding to higher sintering temperatures of the electrode. In contrast, Fig. 8(b) shows a decrease in polarization resistance with increasing measurement temperature.

Various electrical parameters have been derived from the measured impedance data using ZView software, and the results are illustrated in Fig. 9. As shown in Fig. 9(a), the total polarization resistance of BSCF increases with increasing sintering temperature of the electrode. Additionally, the micrographs in Fig. 7 indicate that the porosity of the electrode sintered at 1100 °C for 2 h is lower than that of the electrode sintered at 1000 °C for the same duration. Furthermore, the grain size tends to increase with higher sintering temperatures. Consequently, it is reasonable to anticipate that the electrode sintered at 1100 °C will demonstrate lower polarization resistance, in line with the previously discussed concepts of electrical conductivity. Observations indicate that the polarization resistance of the electrode sintered at 1100 °C is greater than that of the electrode sintered at 1000 °C. This discrepancy can be attributed to the chemical stability of the BSCF electrode in conjunction with SDC electrolytes. At the higher sintering temperature of 1100 °C, BSCF may react with the SDC buffer layer, producing insulating impurity phases. The presence of these intermediate compounds has contributed to the rise in polarization resistance[29].

The results depicted in Fig. 9(b) and (c) highlight that a significant reduction in diffusion resistance ($R_2$) is a vital factor in decreasing $R_p$. $R_2$ is connected to the diffusion of oxygen ions. Oxygen diffusion is hindered by porosity and grain boundaries. As the electrode sintering temperature increases, porosity decreases, and grain size increases; oxygen-ion diffusion should increase, and $R_2$ should decrease. However, the current research indicates that $R_2$ values increase with higher sintering temperatures of the electrode. The elevated $R_2$ observed in samples sintered at 1100 °C may be due to the reaction between BSCF and the SDC electrolyte, resulting in the formation of intermediate phases[29].

Activation energy for oxygen diffusion was calculated from the Arrhenius plots of $R_2$ for BSCF samples, yielding 86.94 and 104.22 kJ/mol for electrodes sintered at 1000 and 1100 °C, respectively. This rise in activation energy with higher sintering temperatures is attributed to the formation of intermediate phases resulting from the elevated sintering conditions of the electrodes[29].

The capacitance ($C_i$) for each electrode process, required for understanding the oxygen reduction process, is calculated using the following equation[39]:

$$C_i = \frac{(R_i Q_i)^{\frac{1}{n_i}}}{R_i} \quad \ldots (7)$$

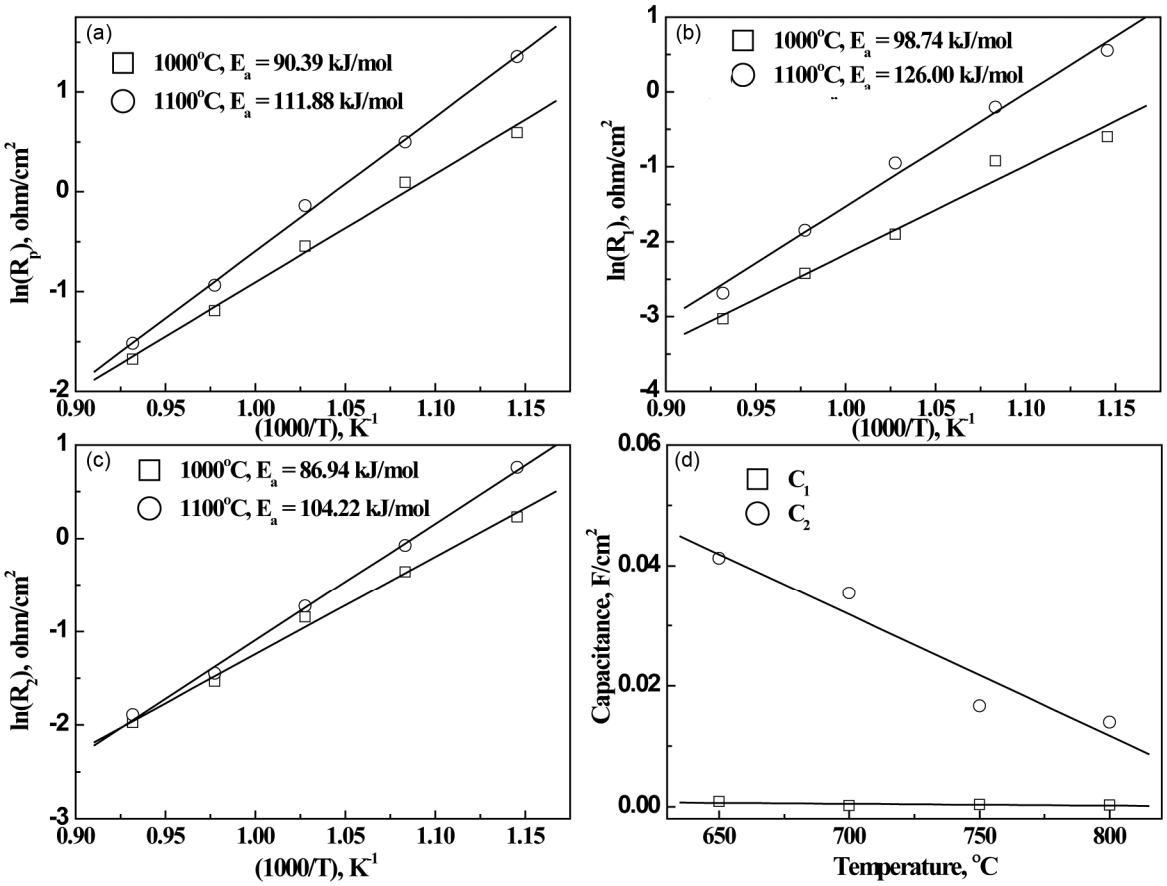


Fig. 9 — Temperature dependent electrode polarization contributions of BSCF electrode on SDC buffer layered YSZ electrolyte: (a) polarization resistance $R_p$, (b) charge transfer resistance $R_1$, (c) diffusion resistance $R_2$, and (d) capacitance

where $C_i$ = interfacial capacitance, $Q_i$ = constant phase element representing time-dependent capacitive elements, $R_i$ = cathode polarization resistance, and $n_i = Q_i$'s similarity to a true capacitor of the individual electrode processes. The capacitance of the BSCF electrode, sintered at 1000 °C for 2 h for each method, is depicted in Fig. 9(d) as a function of temperature. The measured low value of $C_1$ ($10^{-4}$ F/cm$^2$) may be due to oxygen-ion and electron-transfer processes, while the values of $C_2$ (in the order of $10^{-2}$ F/cm$^2$) decrease with increasing temperature, which may be related to molecular oxygen dissociation and diffusion processes[39]. It could be noted that the capacitance ($C_1$) remains independent of temperature as it is related to the delay in electron/ion transfer.

The exchange current density, $i_0$, crucial to understand the oxygen reduction reaction at the cathode, is calculated using the following equation[9]:

$$i_0 = \frac{1}{R_p}\frac{RT\nu}{nF} \quad \ldots (8)$$

Table 1 — Exchange current density $i_0$ (mA/cm$^2$) of BSCF at different temperatures

| Sintering temperature (°C) | Measurement temperature (°C) | | | |
|---|---|---|---|---|
| | 550 | 600 | 650 | 700 |
| | Exchange current density $i_0$ (mA/cm$^2$) | | | |
| 1000 | 4.56 | 12.23 | 19.08 | 34.39 |
| 1100 | 1.04 | 2.5 | 11.33 | 22.91 |

where R = gas constant, v = number of times the rate-determining step occurs for one occurrence of the full reaction, n = total number of electrons passed in the reaction, and F = Faraday constant. Table 1 show that the $i_0$ value for samples sintered at different temperatures for 2 h increases with increasing measurement temperature. This may be due to the increase in diffusivity with temperature.

**Chemical compatibility of SDC with BSCF**

For the study of chemical compatibility of BSCF powder with SDC electrolyte, these two powders were mixed properly in equal weight ratios and then

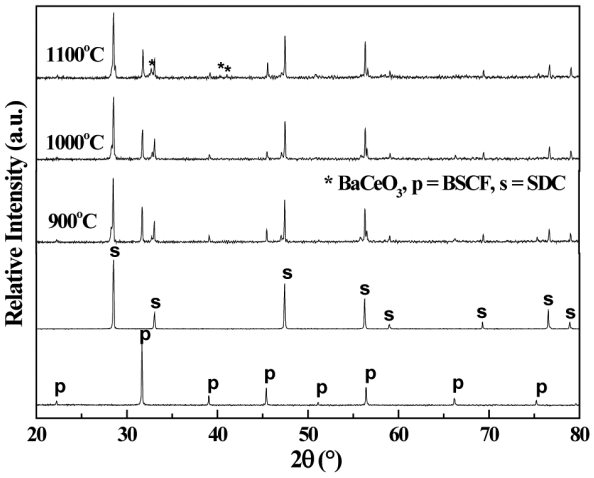


Fig. 10 — XRD patterns of BSCF-SDC composite powder as a function of calcination temperature

calcined at temperatures between 900 and 1100 °C for 8 h. XRD pattern of these calcined powders and the individual powders are presented in Fig. 10. The analysis revealed that the mixed powder exhibited only two distinct phases (BSCF and SDC) when subjected to calcination at temperatures of 900 and 1000 °C with no other impurity phases present. Calcination at 1110 °C revealed the presence of $BaCeO_3$, in addition to the BSCF and SDC phases. This indicated the reaction between BSCF and SDC at high temperatures, leading to the formation of secondary phases and thus validates our assumption[37].

## Conclusion

BSCF sintered at 1100 °C for 8 h shows a well-indexed cubic perovskite structure with a lattice parameter of 3.9939 Å. The nonlinear thermal expansion behaviour of the BSCF sample could be well explained by considering defect chemistry and the temperature-dependent weight loss behaviour. The specific TEC values are 12.99, 22.48, and 17.48 ($\times 10^{-6}$/K) over the temperature ranges 30 to 300, 300 to 500, and 30 to 800 °C, respectively. The calculated average grain size of BSCF sintered at 1100 °C is 8.88±1.3, 11.84±2.2, and 14.76±2.6 μm for soaking times of 2, 4, and 8 h, respectively. The peak conductivity of the BSCF samples sintered at 1100 °C for soaking periods of 4 and 8 h are 40.25 and 44.85 S/cm, respectively. Activation energies of BSCF samples below 300 °C are found to be between 33.74 and 39.14 kJ/mol. Impedance spectroscopy indicates that the polarization resistance and other electrochemical parameters are strongly influenced by the sintering profile. BSCF electrode sintered at 1100 °C shows interconnected large grains with porosity along the grain junctions. Activation energies of 86.94 and 104.22 kJ/mol are found for the BSCF electrodes sintered at 1000 and 1100 °C, respectively. The electrode sintered at 1000 °C shows the lowest polarization resistance. Capacitance $C_1$ is found to be in the order of $10^{-4}$ F/cm$^2$ and $C_2$ in the order of $10^{-2}$ F/cm$^2$. The exchange current density of the BSCF samples sintered at 1000 °C for 2 h increases from 4.56 to 34.39 mA/cm$^2$ as the measurement temperature increases from 550 to 700 °C. The BSCF-SDC powder mixture shows two phases (BSCF and SDC) when calcined at 1000 °C, whereas at 1100 °C, an impurity is observed.

## Acknowledgements

One of the authors, Hemalata Patra, acknowledges the National Institute of Technology, Rourkela, Odisha, India, for providing the necessary research facilities.

## Conflict of Interest

The authors declare no conflicts of interest.

## References

1 Singh S K & Kumar J, AC conductivity, dielectric losses, permittivity behavior of $Ba_xSr_{1-x}Fe_{0.8}Co_{0.2}O_{3-\delta}$ (x = 0, 0.5 and 1) ceramics, *J Mater Sci*, 42 (2007) 2105.

2 Yang Z, Harvey A S, Infortuna A, Schoonman J & Gauckler L J, Electrical conductivity and defect chemistry of $Ba_xSr_{1-x}Co_yFe_{1-y}O_{3-\delta}$ perovskites, *J Solid State Electrochem*, 15 (2011) 277.

3 Ahmadrezaei M, Muchtar A, Muhamad N, Tan C Y & Majlan E H, Electrochemical and microstructural characteristics of nanoperovskite oxides $Ba_{0.2}Sr_{0.8}Co_{0.8}Fe_{0.2}O_{3-\delta}$ (BSCF) for solid oxide fuel cells, *Ceram Int*, 39 (2013) 439.

4 Jun A, Yoo S, Gwon O, Shin J & Kim G, Thermodynamic and electrical properties of $Ba_{0.5}Sr_{0.5}Co_{0.8}Fe_{0.2}O_{3-\delta}$ and $La_{0.6}Sr_{0.4}Co_{0.2}Fe_{0.8}O_{3-\delta}$ for intermediate-temperature solid oxide fuel cells, *Electrochim Acta*, 89 (2013) 372.

5 Zhou W, Ran R, Shao Z, Jin W & Xu N, Evaluation of a site cation-deficient $(Ba_{0.5}Sr_{0.5})_{1-x}Co_{0.8}Fe_{0.2}O_{3-\delta}$(x>0) perovskite as a solid-oxide fuel cell cathode, *J Power Sources*, 182 (2008) 24.

6 Ge L, Zhou W, Ran R, Liu S, Shao Z, Jin W & Xu N, Properties and performance of a site deficient $(Ba_{0.5}Sr_{0.5})_{1-x}Co_{0.8}Fe_{0.2}O_{3-\delta}$ for oxygen permeating membrane, *J Membr Sci*, 306 (2007) 318.

7 Kostogloudis G C & Ftikos C, Properties of A-site-deficient $La_{0.6}Sr_{0.4}Co_{0.2}Fe_{0.8}O_{3-\delta}$ based perovskite oxides, *Solid State Ion*, 126 (1999) 143.

8 Baumann F S, Fleig J, Habermeier H U & Maier J, $Ba_{0.5}Sr_{0.5}Co_{0.8}Fe_{0.2}O_{3-\delta}$ thin film microelectrodes investigated by impedance spectroscopy, *Solid State Ion*, 177 (2006) 3187.

9 Liu B, Zhang Y & Zhang L, Oxygen reduction mechanism at $Ba_{0.5}Sr_{0.5}Co_{0.8}Fe_{0.2}O_{3-\delta}$ cathode for solid oxide fuel cell, *Int J Hydrog Energy*, 34 (2009) 1008.

10 Azad U P, Singh M, Ghosh S, Singh A K, Ganesan V, Singh A K & Prakash R, Facile synthesis of BSCF perovskite oxide as an efficient bifunctional oxygen electrocatalyst, *Int J Hydrog Energy*, 43 (2018) 20671.

11 Ahmad M Z, Ahmad S H, Chen R S, Ismail A F, Hazan R & Baharuddin N A, Review on recent advancement in cathode material for lower and intermediate temperature solid oxide fuel cells application, *Int J Hydrog Energy*, 47 (2022) 1103.

12 Vente J F, McIntosh S, Haije W G & Bouwmeester H J M, Properties and performance of $Ba_xSr_{1-x}Co_{0.8}Fe_{0.2}O_{3-\delta}$ materials for oxygen transport membranes, *J Solid State Electrochem*, 10 (2006) 581.

13 Zhu Q, Jin T & Wang Y, Thermal expansion behavior and chemical compatibility of $Ba_xSr_{1-x}Co_{1-y}Fe_yO_{3-\delta}$ with 8YSZ and 20GDC, *Solid State Ion*, 177 (2006) 1199.

14 Zhou W, Ran R & Shao Z, Progress in understanding and development of $Ba_{0.5}Sr_{0.5}Co_{0.8}Fe_{0.2}O_{3-\delta}$-based cathodes for intermediate-temperature solid-oxide fuel cells: A review, *J Power Sources*, 192 (2009) 231.

15 Lee S, Lim Y, Lee E A, Hwang H J & Moon J W, $Ba_{0.5}Sr_{0.5}Co_{0.8}Fe_{0.2}O_{3-\delta}$ (BSCF) and $La_{0.6}Ba_{0.4}Co_{0.2}Fe_{0.8}O_{3-\delta}$ (LBCF) cathodes prepared by combined citrate-EDTA method for IT-SOFCs, *J Power Sources*, 157 (2006) 848.

16 Duan Z, Yang M, Yan A, Hou Z, Dong Y, Chong Y, Cheng M & Yang W, $Ba_{0.5}Sr_{0.5}Co_{0.8}Fe_{0.2}O_{3-\delta}$ as a cathode for IT-SOFCs with a GDC interlayer, *J Power Sources*, 160 (2006) 57.

17 Wang H, Tablet C, Feldhoff A & Caro J, Investigation of phase structure, sintering, and permeability of perovskite-type $Ba_{0.5}Sr_{0.5}Co_{0.8}Fe_{0.2}O_{3-\delta}$ membranes, *J Membr Sci*, 262 (2005) 20.

18 Qiu L, Ichikawa T, Hirano A, Imanishi N & Takeda Y, $Ln_{1-x}Sr_xCo_{1-y}Fe_yO_{3-\delta}$ (Ln = Pr, Nd, Gd; x=0.2, 0.3) for the electrodes of solid oxide fuel cells, *Solid State Ion*, 158 (2003) 55.

19 Ivers-Tiffee E, Weber A & Herbstritt D, Materials and technologies for SOFC-components, *J Eur Ceram Soc*, 21 (2001) 1805.

20 Teraoka Y, Zhang H M, Okamoto K & Yamazoe N, Mixed ionic-electronic conductivity of $La_{1-x}Sr_xCo_{1-y}Fe_yO_{3-\delta}$ perovskite-type oxides, *Mater Res Bull*, 23 (1988) 51.

21 Shao Z & Haile S M, A high-performance cathode for the next generation of solid-oxide fuel cells, *Nature*, 431 (2004) 170.

22 Caneiro A, Mogni L, Grunbaum N & Prado F, Physicochemical properties of non-stoichiometric oxides Mixed conductors: Part I, *J Therm Anal Calorim*, 103 (2011) 597.

23 Sun C, Hui R & Roller J, Cathode materials for solid oxide fuel cells: A review, *J Solid State Electrochem*, 14 (2010) 1125.

24 Jiang S P, Development of lanthanum strontium manganite perovskite cathode materials of solid oxide fuel cells: A review, *J Membr Sci*, 43 (2008) 6799.

25 Murray E P, Tsai T & Barnett S A, Oxygen transfer processes in $(La,Sr)MnO_3/Y_2O_3$-stabilized $ZrO_2$ cathodes: An impedance spectroscopy study, *Solid State Ion*, 110 (1998) 235.

26 Rout S K, Patra H, Bhattacharyya S & Pratihar S K, Grain size dependent thermal and electrical behaviour of $La_{0.6}Sr_{0.4}Co_{0.2}Fe_{0.8}O_{3-\delta}$, *Integr Ferroelectr*, 185 (2017) 52.

27 Yang Z, Guo M, Wang N, Ma C, Wang J & Han M, A short review of cathode poisoning and corrosion in solid oxide fuel cell, *Int J Hydrog Energy*, 42 (2017) 24948.

28 Zhu Y, Wu M, Liu J, Jia D, Tan J, Zhang G, Liu Z, Liu G & Jin W, Binary-halogen doped BSCF oxide provides ahighly oxygen permeable membrane, *J Membr Sci*, 717 (2025) 123654.

29 Patra H, Rout S K, Pratihar S K & Bhattacharya S, Thermal, electrical and electrochemical characteristics of $Ba_{1-x}Sr_x\ Co_{0.8}Fe_{0.2}O_{3-\delta}$ cathode material for intermediate temperature solid oxide fuel cells, *Int J Hydrog Energy*, 36 (2011) 11904.

30 Toprak M S, Darab M, Syvertsen G E & Muhammed M, Synthesis of nanostructured BSCF by oxalate co-precipitation: As potential cathode material for solid oxide fuels cells, *Int J Hydrog Energy*, 35 (2010) 9448.

31 Zeng P, Chen Z, Zhou W, Gu H, Shao Z & Liu S, Re-evaluation of $Ba_{0.5}Sr_{0.5}Co_{0.8}Fe_{0.2}O_{3-\delta}$ perovskite as oxygen semi-permeable membrane, *J Membr Sci*, 291 (2007) 148.

32 McIntosh S, Vente J F, Haije W G, Blank D H A & Bouwmeester H J M, Structure and oxygen stoichiometry of $SrCo_{0.8}Fe_{0.2}O_{3-\delta}$ and $Ba_{0.5}Sr_{0.5}Co_{0.8}Fe_{0.2}O_{3-\delta}$, *Solid State Ion*, 177 (2006) 1737.

33 Kim Y M, Kim-Lohsoontorn P, Baek S W & Bae J, Electrochemical performance of unsintered $Ba_{0.5}Sr_{0.5}\ Co_{0.8}Fe_{0.2}O_{3-\delta}$, $La_{0.6}Sr_{0.4}Co_{0.8}Fe_{0.2}O_{3-\delta}$, and $La_{0.8}\ Sr_{0.2}MnO_{3-\delta}$ cathodes for metal-supported solid oxide fuel cells, *Int J Hydrog Energy*, 36 (2011) 3138.

34 Tan L, Gu X, Yang L, Zhang L, Wang C & Xu N, Influence of sintering condition on crystal structure, microstructure, and oxygen permeability of perovskite-related type $Ba_{0.8}Sr_{0.2}\ Co_{0.8}Fe_{0.2}O_{3-\delta}$ membranes, *Sep Purif Technol*, 32 (2003) 307.

35 Tan L, Gu X, Yang L, Jin W, Zhang L & Xu N, Influence of powder synthesis methods on microstructure and oxygen permeation performance of $Ba_{0.5}Sr_{0.5}Co_{0.8}Fe_{0.2}O_{3-\delta}$ perovskite-type membranes, *J Membr Sci*, 212 (2003) 157.

36 Badwal S P S & Foger K, Solid oxide electrolyte fuel cell review, *Ceram Int*, 22 (1996) 257.

37 Patra H, Studies on Sr/Co substituted barium ferrite materials for IT-SOFCs cathode applications, Ph.D. thesis, National Institute of Technology, Rourkela, (2012).

38 Patra H, Rout S K, Pratihar S K & Bhattacharya S, Effect of process parameters on combined EDTA-citrate synthesis of $Ba_{0.5}Sr_{0.5}Co_{0.8}Fe_{0.2}O_{3-\delta}$ perovskite, *Powder Technol*, 209 (2011) 98.

39 Ding X, Kong X, Jiang J, Cui C & Guo X, Characterization and electrochemical performance of $(Ba_{0.6}Sr_{0.4})_{1-x}La_x\ Co_{0.6}Fe_{0.4}\ O_{3-\delta}$(x = 0, 0.1) cathode for intermediate temperature solid oxide fuel cells, *Mater Res Bull*, 45 (2010) 1271.

40 Li S, Lu Z, Huang X, Wei B & Su W, Thermal, electrical, and electrochemical properties of Lanthanum-doped $Ba_{0.5}Sr_{0.5}\ Co_{0.8}Fe_{0.2}O_{3-\delta}$, *J Phys Chem Solids*, 68 (2007) 1707.

41 Huang B X, Malzbender J, Steinbrech R W & Singheiser L, Discussion of the complex thermo-mechanical behavior of $Ba_{0.5}Sr_{0.5}Co_{0.8}Fe_{0.2}O_{3-\delta}$, *J Membr Sci*, 359 (2010) 80.

42 Shao Z, Xiong G, Tong J, Dong H &Yang W, Ba effect in doped $Sr(Co_{0.8}Fe_{0.2})O_{3-\delta}$ on the phase structure and oxygen permeation properties of the dense ceramic membranes, *Sep Purif Technol*, 25 (2001) 419.

43 Stevenson J W, Armstrong T R, Carneim R D, Pederson L R & Weber W J, Electrochemical properties of mixed conducting perovskites $La_{1-x}M_xCo_{1-y}Fe_yO_{3-\delta}$ (M = Sr, Ba, Ca), *J Electrochem Soc*, 143 (1996) 2722.

44 Huang C Y & Huang T J, Effect of Co substitution for Mn on $Y_{1-x}Sr_xMnO_3$ properties for SOFC cathode material, *J Mater Sci*, 37 (2002) 4581.

45 Zhou W, Ran R, Shao Z, Zhuang W, Jia J, Gu H, Jin W & Xu N, Barium-and strontium-enriched $(Ba_{0.5}Sr_{0.5})_{1+x}Co_{0.8}Fe_{0.2}O_{3-\delta}$ oxides as high-performance cathodes for intermediate-temperature solid-oxide fuel cells, *Acta Mater*, 56 (2008) 2687.